

AD-A161 220

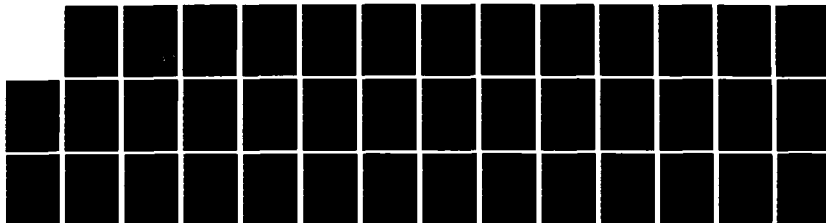
KINETICS OF THE H2-WF2 SYSTEM(U) AEROSPACE CORP EL
SEGUNDO CA J B KOFFEND ET AL. 28 SEP 85
TR-0004A(9990)-2 SD-TR-85-55 F04701-83-C-0004

1/1

UNCLASSIFIED

F/G 7/5

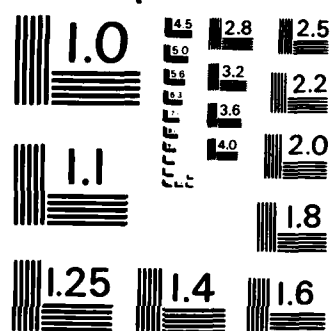
NL



END

FBI/DOJ

011



MICROCOPY RESOLUTION TEST CHART
NATIONAL BUREAU OF STANDARDS-1963-A

AD-A161 220

Kinetics of the H_2-NF_2 System

J. B. KOFFEND, C. E. GARDNER,
and R. F. HEIDNER III
Aerophysics Laboratory
Laboratory Operations
The Aerospace Corporation
El Segundo, Calif. 90245

28 September 1985

APPROVED FOR PUBLIC RELEASE;
DISTRIBUTION UNLIMITED

Prepared for
AIR FORCE WEAPONS LABORATORY
Kirtland Air Force Base, NM 87117

DTIC FILE COPY

SD
DTIC
ELECTE
NOV 18 1985
E


SPACE DIVISION
AIR FORCE SYSTEMS COMMAND
Los Angeles Air Force Station
P.O. Box 92960, Worldway Postal Center
Los Angeles, CA 90009-2960

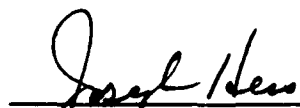
85 11 12 008

This report was submitted by The Aerospace Corporation, El Segundo, CA 90245, under Contract No. F04701-83-C-0084 with the Space Division, P.O. Box 92960, Worldway Postal Center, Los Angeles, CA 90009-2960. It was reviewed and approved for The Aerospace Corporation by W. P. Thompson, Director, Aerophysics Laboratory. 2nd Lt Scott W. Levinson, SD/YNS, was the Air Force Project Officer.

This report has been reviewed by the Public Affairs Office (PAS) and is releasable to the National Technical Information Service (NTIS). At NTIS, it will be available to the general public, including foreign nationals.

This technical report has been reviewed and is approved for publication. Publication of this report does not constitute Air Force approval of the report's findings or conclusions. It is published only for the exchange and stimulation of ideas.


Scott W. Levinson, 2nd Lt, USAF
Project Officer


Joseph Hess, GM-15, Director, West Coast
Office, AF Space Technology Center

REPORT DOCUMENTATION PAGE		READ INSTRUCTIONS BEFORE COMPLETING FORM	
1. REPORT NUMBER SD-TR-85-55	2. GOV ACCESSION NO. AD A161220	3. RECIPIENT'S CATALOG NUMBER	
4. TITLE (and Subtitle) KINETICS OF THE H_2 - NF_2 SYSTEM		5. TYPE OF REPORT & PERIOD COVERED	
		6. PERFORMING ORG. REPORT NUMBER TR-0084A(9990)-2	
7. AUTHOR(s) J. Brooke Koffend, Carrol E. Gardner, and Raymond F. Heidner III		8. CONTRACT OR GRANT NUMBER(s) F04701-83-C-0084	
9. PERFORMING ORGANIZATION NAME AND ADDRESS The Aerospace Corporation El Segundo, CA 90245		10. PROGRAM ELEMENT, PROJECT, TASK AREA & WORK UNIT NUMBERS	
11. CONTROLLING OFFICE NAME AND ADDRESS Air Force Weapons Laboratory Kirtland Air Force Base, NM 87117		12. REPORT DATE 28 September 1985	
		13. NUMBER OF PAGES 35	
14. MONITORING AGENCY NAME & ADDRESS (if different from Controlling Office) Space Division Los Angeles Air Force Station Los Angeles, CA 90009-2960		15. SECURITY CLASS. (of this report) Unclassified	
		15a. DECLASSIFICATION/DOWNGRADING SCHEDULE	
16. DISTRIBUTION STATEMENT (of this Report) Approved for public release; distribution unlimited.			
17. DISTRIBUTION STATEMENT (of the abstract entered in Block 20, if different from Report)			
18. SUPPLEMENTARY NOTES			
19. KEY WORDS (Continue on reverse side if necessary and identify by block number) Chemical Lasers, N_2F_4 Electronically Excited States, NF_2 Laser Photochemistry, Time-Resolved Kinetics, H_2 Sq. Molecule Cm to the 6th Power			
20. ABSTRACT (Continue on reverse side if necessary and identify by block number) The reaction of hydrogen atoms with NF_2 was studied in a flow tube using pulsed KrF laser initiation of $H_2/NF_2/Ar$ mixtures at 440 K. The quantum yield for $NF(a)$ production from the 249 nm photolysis of NF_2 was determined to be 0.10 ± 0.05 . Several important reactions in this system were investigated, and rate coefficients were determined at 440 K. A value of $(1.03 \pm 0.20) \times 10^{-30} \text{ cm}^6/\text{molecule}^2\text{-sec}$ was obtained for the three-body recombination of F atoms with NF_2 and Ar. Rate constants for the relaxation			

UNCLASSIFIED

SECURITY CLASSIFICATION OF THIS PAGE(When Data Entered)

19. KEY WORDS (Continued)

20. ABSTRACT (Continued)

of HF($v = 2$) and HF($v = 3$) by NF_2 are $(9.7 \pm 1.0) \times 10^{-14}$ and $(2.5 \pm 0.5) \times 10^{-13} \text{ cm}^3/\text{molecule-sec}$, respectively. Study of the quenching of $\text{NF}(a)$ by NF_2 yields a rate coefficient of $(2.7 \pm 1.0) \times 10^{-16} \text{ cm}^3/\text{molecule-sec}$. Evidence is presented that indicates the disproportionation of $\text{NF}(a)$ is three orders of magnitude slower than that of ground state NF . Modeling results are presented which agree well with experimental data.

UNCLASSIFIED

SECURITY CLASSIFICATION OF THIS PAGE(When Data Entered)

PREFACE

The authors wish to thank Dr. R. L. Wilkins for his help in the construction of the analytic model. Dr. J. V. V. Kasper is gratefully acknowledged for his aid in developing the data acquisition system. We thank Drs. N. Cohen and K. Westberg for fruitful discussions on the three-body recombination of NF_2 and F atoms. We are indebted to Dr. J. M. Herbelin for his help with the understanding of the chemistry and handling of N_2F_4 .

Accession For	
NTIS GRA&I	<input checked="" type="checkbox"/>
DTIC TAB	<input type="checkbox"/>
Unannounced	<input type="checkbox"/>
Justification	
By _____	
Distribution/	
Availability Codes	
Avail and/or	
Dist	Special
A-1	



CONTENTS

PREFACE.....	1
I. INTRODUCTION.....	7
II. EXPERIMENTAL.....	9
III. RESULTS AND DISCUSSION.....	13
A. Photochemistry of NF_2	13
B. Three-Body Recombination of F with NF_2	20
C. Computer Model of the NF_2/H_2 System.....	26
D. NF(a) Quantum Yield.....	31
IV. CONCLUSIONS.....	33
REFERENCES.....	35
APPENDIX A - NF(a) KINETIC MODEL.....	37
APPENDIX B - REACTIONS USED IN THE NEST MODEL.....	41

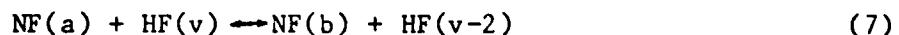
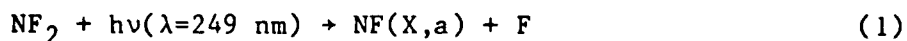
FIGURES

1.	Diagram of the Experimental Apparatus.....	10
2.	NF a-X Emission Time Profile from the KrF Photolysis of NF ₂ in Ar.....	14
3.	HF v = 3 → v = 1 Emission Time Profile from the KrF Photolysis of NF ₂ in Ar.....	16
4a.	HF(v' → v'-2) Emission Decays as a Function of NF ₂ Density.....	17
4b.	HF(v' → v'-2) Emission Inverse Risetimes as a Function of HF ₂ Density.....	18
5.	NF a → X Fluorescence Decay from Photolysis of NF ₂ /Ar Mixtures vs. [NF ₂].....	21
6.	NF a-X Emission Decay as a Function of [NF(a)].....	22
7.	Plot of NF(a) Amplitudes vs. [Ar] According to Eq. (3).....	25
8.	Plot of NF(a) Amplitudes vs. [H ₂] According to Eq. (4).....	27
9.	Formation Behavior of NF(a) from KrF Photolysis of an NF ₂ /H ₂ /Ar Mix.....	29
10.	NF(a) Amplitudes as a Function of [H ₂].....	30
11.	NF(a) Risetimes as a Function of [H ₂].....	32

PREVIOUS PAGE
IS BLANK

I. INTRODUCTION

The reactions of NF_2 and NF radicals with various atoms and molecules have been examined in several studies.¹⁻¹⁷ Reaction systems involving NF_2 or NF are among the few that efficiently produce electronically excited products. These systems have sparked interest because of their potential use in chemically pumped lasers. In this work, we investigated the kinetics of the reactions initiated by excimer laser photolysis of NF_2 in the presence of H_2 . The important processes under our experimental conditions include:



This system is important since it serves as an efficient chemical source of the metastable $\text{NF}(\text{a})$ radical. Reaction (4) is known to produce the $\text{NF}(\text{a})$ state with a branching ratio in excess of 0.9.¹⁶ Because of the rapid disproportionation of $\text{NF}(\text{X})$ in reaction (5)¹⁴, which regenerates fluorine atoms, a chain reaction occurs under certain experimental conditions. Hence, this system has been of interest as a chemical source of a metastable species, which could be used as an energy donor in a collisionally pumped chemical laser. The goal in this study was to characterize the important reactions

and processes produced from the pulsed KrF laser initiation of $\text{NF}_2/\text{H}_2/\text{Ar}$ mixtures. There are several advantages obtained using this method over conventional flow-tube studies. Since the species that initiate the chemistry are generated by the KrF photolysis pulse, homogeneity can be obtained by premixing reactants and precursors. Hence, the chemistry and energy transfer can be separated from the mixing process. The short and relatively high-intensity KrF pulse (~ 200 mJ in 15 nsec) permits the generation of high densities of photolysis products with a precise time origin. The ability to obtain high densities allows the study of second order processes such as radical-radical reactions and energy pooling processes.

The quantum yield for NF(a) formation from the photolysis of NF_2 by a KrF laser operating at 249 nm was measured. The quenching of NF(a) and $\text{HF}(v = 2,3)$ by NF_2 was investigated. In addition, an analytic model for the formation of NF(a) valid for conditions of high $[\text{H}_2]/[\text{F}]$ and high $[\text{NF}_2]/[\text{H}]$ ratio was derived. This model permitted the extraction of the value of k_3 from experimental data. This reaction system was also numerically modeled; both the analytic and the numerical models are in good agreement with the experimental data.

II. EXPERIMENTAL

The experimental setup is shown in Fig. 1. A Lambda Physik model EMG 101 excimer laser oscillating at 249 nm with KrF is directed into the photolysis cell with a 45-deg high reflector. In some experiments, the KrF laser was placed such that its axis was coincident with that of the flow cell, and the 45-deg mirror was not used. A beam shaping cylindrical lens or set of lenses could be inserted in the beam prior to entry into the cell. In most experiments, the KrF beam was expanded to fill the cell cross-section as fully as possible with a 6-in. focal-length cylindrical quartz lens in order to minimize the effects of diffusion. The laser was operated with repetition rates of 0.1 to 1 Hz to allow sufficient time between pulses for replacement of the gas mixture in the photolysis cell and to ensure that slow reactions initiated by the laser had terminated. The laser power was measured using a Scientech calorimeter with a 4-in. dia. aperture. Variation of the input optics resulted in photon fluxes as high as 2×10^{18} photons/cm² under focused conditions and as low as 5×10^{15} photons/cm². Further attenuation could be obtained by insertion of a stack of quartz windows in the beam. The KrF laser pulse widths were typically 15 nsec in duration.

The 60-cm long photolysis cell is constructed of quartz and has an i.d. of 4.5 cm. The gases used in these studies were Ar (Matheson 99.9995%), CO₂ (Matheson 99.99%), N₂F₄ (Hercules 96%), and an H₂/Ar mixture (10.14% H₂, 89.86% Ar). In some experiments the Ar was passed at atmospheric pressure through Linde 5A molecular sieve traps, which had been baked at 200°C under vacuum. Flow rates were measured for all gases, except N₂F₄, using Tylan flowmeters that had been calibrated under our experimental conditions by pressure rise versus time in the same calibrated volume. A 10% N₂F₄/Ar mixture was prepared and stored at 90 psia in a 4-liter stainless-steel cylinder. Ar gas and the 10% N₂F₄ mixture were combined in a mixing block and flowed through a quartz bulb maintained at 210°C into the photolysis cell, which was enclosed in an oven and maintained at 170°C. This procedure ensured that the N₂F₄ was 99% dissociated into NF₂.¹⁷⁻²¹ The N₂F₄ mix and the Ar were passed

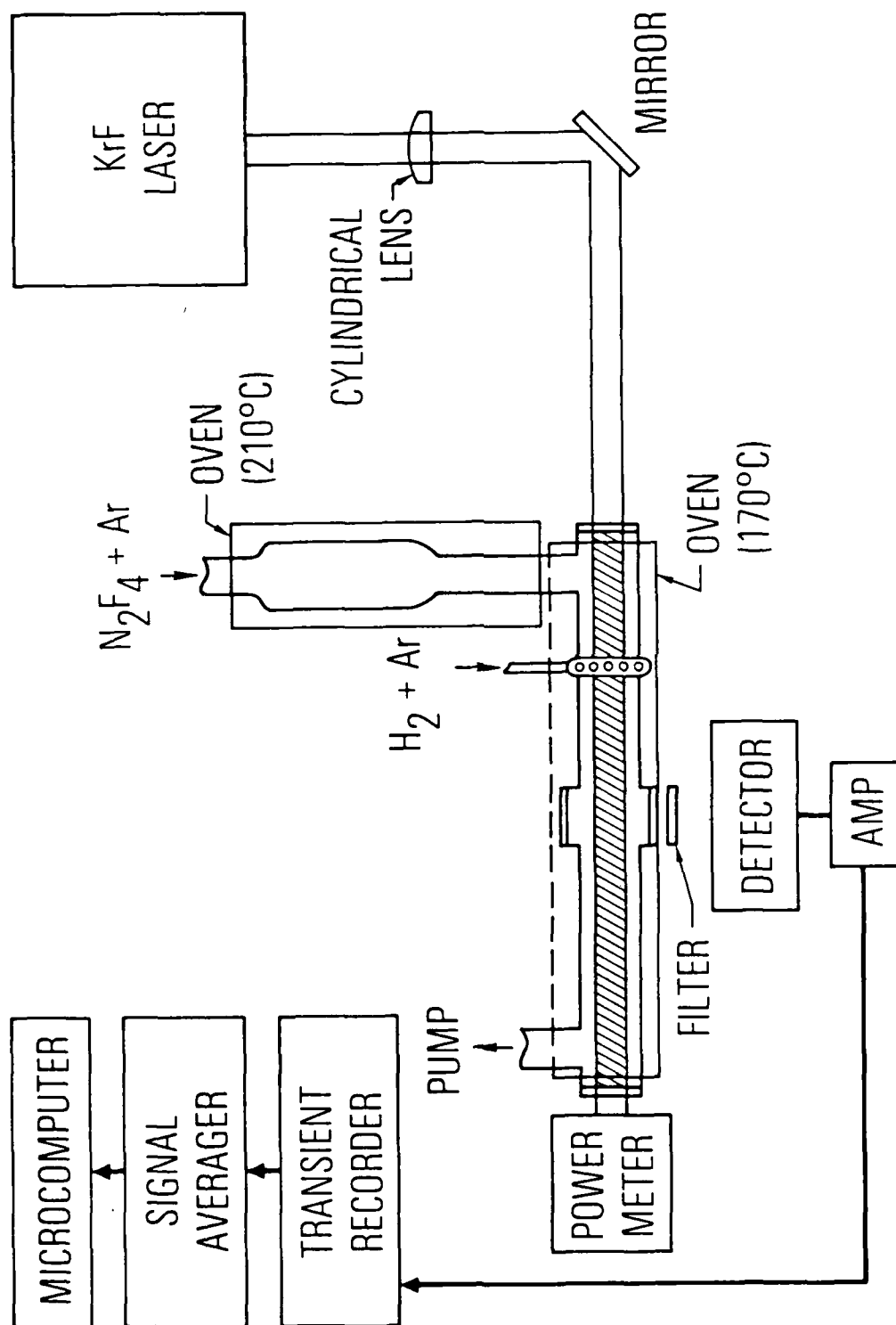


Fig. 1. Diagram of the Experimental Apparatus

through two sonic orifices in the mixing block, and the backing pressure of each was measured with Heise and Matheson absolute pressure gauges, respectively. The flow rate of each orifice was calibrated separately and was linear with respect to backing pressure under all experimental conditions. Pressure in the photolysis cell was measured with an MKS Baratron capacitance manometer.

A thermoelectrically cooled GaAs photomultiplier was used with appropriate narrow bandpass filters to monitor the NF(a) and NF(b) states by their fluorescence at 874 and 529 nm, respectively. The HF($v = 2,3$) states were monitored by observation of the HF($v = 2$) \rightarrow HF($v = 0$) and HF($v = 3$) \rightarrow HF($v = 1$) overtone transitions using an intrinsic Ge detector and narrow bandpass filters. A Biomation 805 transient recorder digitized these signals, and up to 32 traces were summed using a Nicolet 1072 signal averager. The averaged sweeps were transferred to a DEC LSI 11/23 computer for data analysis.

Emission spectra from the laser photolysis products were obtained using the GaAs phototube coupled to a McPherson model 218 1/3-m scanning monochromator. These spectra were recorded using a PAR model 160 boxcar integrator, whose output was transferred to the 11/23 computer using an analog-to-digital converter.

To determine the absorption coefficient of NF₂ at 249 nm, the photolysis cell was modified so that a precise NF₂ absorption length was defined. New cell endcaps were constructed from two concentric tubes so that the cell windows penetrated 3 cm into the heated portion of the cell. A dual-beam arrangement was created using quartz windows as beamsplitters, and the absorption of the 249 nm KrF pulse was measured using two closely matched PIN photodiodes. The difference between the two diode signals was displayed on an oscilloscope, and quartz plates used as attenuators were placed in the probe; reference beams were used to obtain a null in the absence of NF₂. Absolute calibration was provided using a stack of three quartz windows whose transmission at 248.5 nm has been previously determined.

III. RESULTS AND DISCUSSION

A. PHOTOCHEMISTRY OF NF₂

The photolysis of NF₂ at 249 nm will produce an NF radical and a fluorine atom. The energetics^{4,16,18,24-26} of the process dictate that only the NF(a) and NF(X) states will be created at this wavelength. Figure 2 shows a typical NF(a) time profile from the photolysis of an NF₂/Ar mixture. The short but finite risetime indicates that the NF(a) is not formed directly but through some secondary process.

Spectra were recorded of the emission from products of the photolysis of NF₂ in Ar to determine if the emission transmitted through the filter represented only the NF a-X transition at 873 nm. Of special concern is the emission from the HF ($v = 3 \rightarrow 0$) overtone, which overlaps the NF a-X band and is also passed through the filter. Low HF($v = 3$) to NF(a) ratios are predicted under our experimental conditions from the photolysis of NF₂/H₂/Ar mixtures by the computer model described in Section IIIC. This was confirmed when spectra were taken using a boxcar integrator with delays of up to 15 msec relative to the KrF pulse. In all cases, the emission spectra could be attributed only to the NF a-X system. Hence, the time profiles obtained with the 873 nm interference filter are caused solely by NF(a).

To our surprise, NF(b) as well as HF($v = 2,3$) was observed under these experimental conditions, i.e., NF₂ in Ar. In an attempt to eliminate the hydrogen bearing impurity implied by this result, the Ar used as diluent and in preparation of the 10% N₂F₄/Ar mixture was passed through molecular sieve traps immersed in a dry ice/methanol bath. The sieves were degassed at 500 K prior to use. However, the NF(b) and HF signals persisted. From examination of the time profiles of the HF overtone emissions, evidence was obtained indicating that the HF is formed from the reaction of fluorine atoms with some hydrocarbon impurity (or possibly HNF₂) rather than from the reaction of hydrogen atoms with NF₂. If one neglects second order processes such as HF(v) + HF(v') \rightarrow HF($v - 1$) + HF($v' + 1$) pooling, the HF emission should display

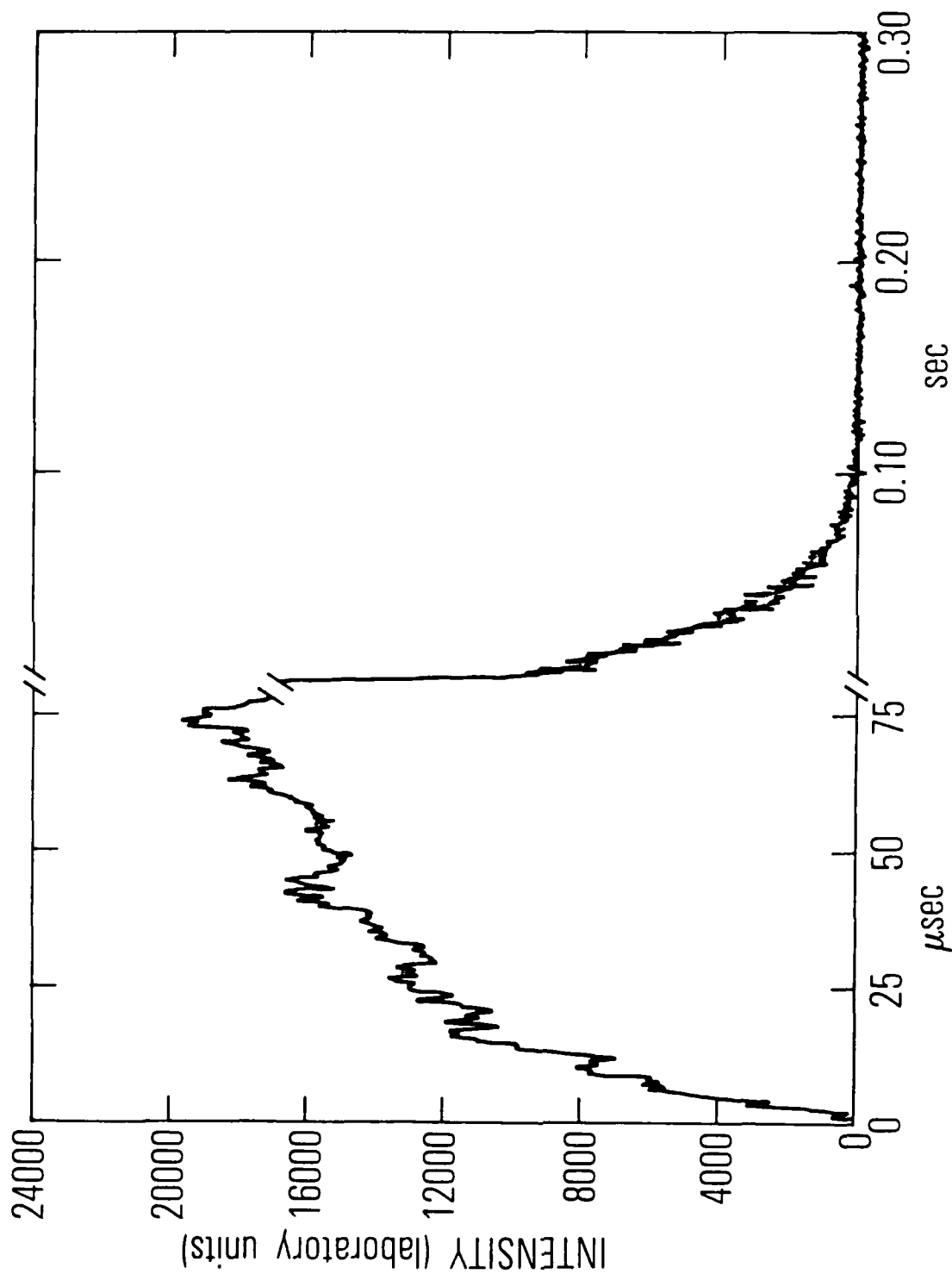


Fig. 2. NF a-X Emission Time Profile from the KrF Photolysis of NF_2 in Ar.
 $[\text{NF}_2]: 9.8 \times 10^{15}$ molecule/ cm^3 , $[\text{Ar}]: 4.0 \times 10^{17}$ molecule/ cm^3 , KrF
 flux: 8×10^{15} photons/ cm^2 (note dual timescales)

double exponential behavior. The rise and fall times will reflect the formation and the quenching rates, and their relative magnitudes will determine which rate governs the rise time and which governs the fall time. A nonlinear least squares routine was used to fit HF($v = 2$) and HF($v = 3$) time profiles to a three-parameter double-exponential function, $HF = a(1) \{e^{-a(2)t} - e^{-a(3)t}\}$, to extract rise and fall times from the data. Typical HF($v = 3$) behavior is shown in Fig. 3. Analysis of HF signals as a function of $[NF_2]$ yields the plots displayed in Figs. 4(a) and 4(b). The slopes of HF($v = 2$) and HF($v = 3$) decay versus $[NF_2]$ agree within experimental error, whereas the slopes from Fig. 4(b) differ by a factor of 2.6 ± 0.7 . Thus, the HF($v = 2,3$) decays reflect the formation rates, and the quenching rates are represented by the risetimes. Rate constants for the quenching of HF($v = 2$) and HF($v = 3$) by NF_2 obtained from Fig. 4(b) are $(9.7 \pm 1.0) \times 10^{-13}$ and $(2.5 \pm 0.5) \times 10^{-13}$ $cm^3/molecule\text{-}sec$, respectively. The ratio of these constants agrees well with the empirical $v^{2.7}$ power law observed in HF vibrational quenching rates,²⁷ lending credence to the assumption that the quenching rate is reflected by the HF risetimes.

To determine the rate constant for the reaction of the F atoms with the hydrogen containing impurity {assuming $[F] > [impurity]$ }, the abscissa in Fig. 4(a) must be replaced by the fluorine atom density. Because of the formation of F from reaction (5), however, the F atom density is not strictly a constant. Nevertheless, the average F density can be estimated from the knowledge of the KrF intensity, of the NF_2 absorption cross section, and of the NF(a) quantum yield to within a factor of 2. A rate constant of $\sim 3 \times 10^{-11}$ $cm^3/molecule\text{-}sec$ is obtained in this manner, which is typical of fluorine abstraction reactions.

Comparison of Figs. 2 and 3 also provides evidence that the aforementioned analysis is valid. If the HF were formed from the reaction of H atoms with NF_2 the NF(a) and HF time profiles would be indicative of the same rate of product formation by reaction (4); this is not the case. In addition, the NF(b) and HF profiles show similar behavior, indicating that the NF(b) is formed from energy pooling in reaction (7) rather than directly from reaction (4).

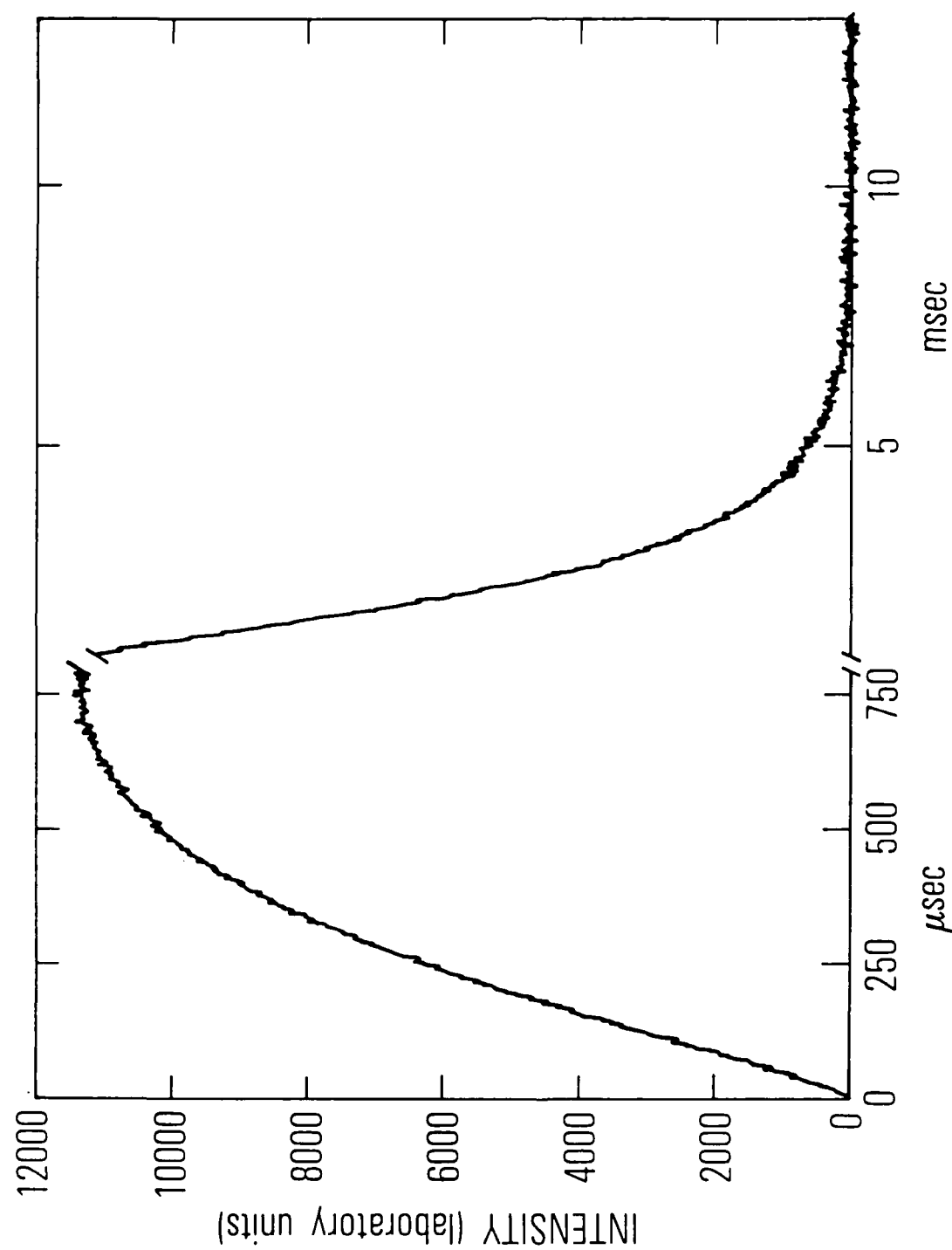


Fig. 3. HF $v = 3 \rightarrow v = 1$ Emission Time Profile from the KrF Photolysis of NF_2 in Ar . $[\text{NF}_2]: 1.4 \times 10^{16}$ molecule/ cm^3 , $[\text{Ar}]: 3.6 \times 10^{17}$ molecule/ cm^3 , KrF flux: 4×10^{15} photons/ cm^2 (note dual timescales)

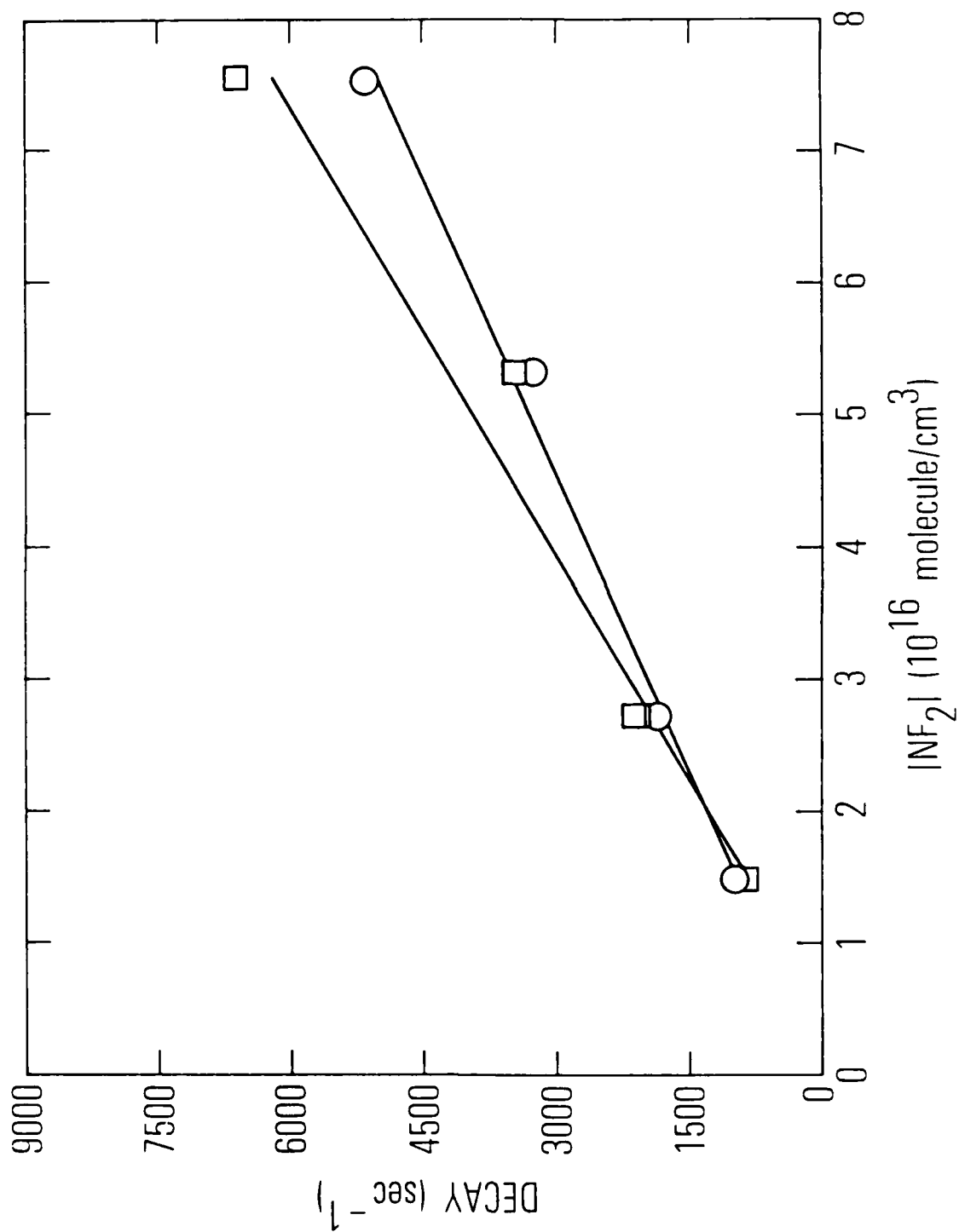


Fig. 4(a). $HF(v' \rightarrow v'-2)$ Emission Decays as a Function of NF_2 Density

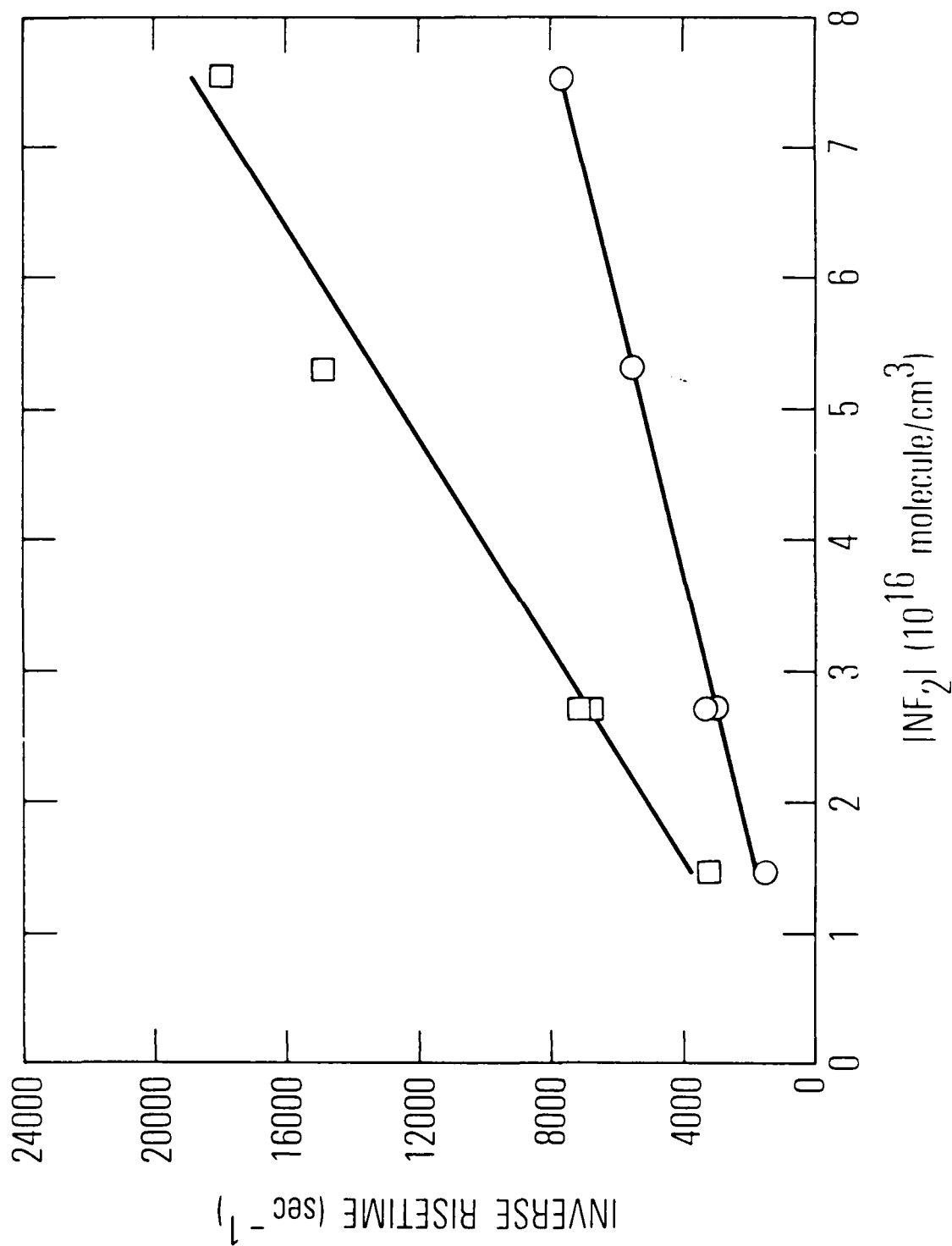


Fig. 4(b). $\text{HF}(v' \rightarrow v'-2)$ Emission Inverse Risettimes as a Function of NF_2 Density. $\text{HF}(v = 2)$ is indicated by the circles, and the squares represent $\text{HF}(v = 3)$. Linear fits to the data are also displayed.

The NF_2 radical exhibits its first absorption band in the UV. This band has a half-width of 20 nm and is peaked near 260 nm.²¹ The diffuse structure observed in this band may indicate that the NF_2 state at 260 nm has some discrete character which would lengthen its lifetime relative to photodissociation in a pure continuum. A similar situation has been observed for ozone excited in the Hartley band.²⁸ The finite risetime of $\text{NF}(a)$ upon 249 nm photolysis of NF_2 may be caused by this discrete state embedded in the continuum.

According to Kuznetsova *et al.*,²² the absorption spectrum of NF_2 shows a marked temperature dependence. In a dual beam experiment described in Section II, we measured the NF_2 absorption coefficient *in situ* using the KrF laser as the light source. The KrF beam was split, and one beam was directed through the cell, whereas the other served as a reference. We verified that the transmission through the cell was inversely proportional to $[\text{NF}_2]$ at a constant temperature. The density of NF_2 in these experiments was in the range $(0.5 - 4.0) \times 10^{16}$ molecule/cm³, which resulted in 91 - 55% transmission for the 22 cm pathlength. We also studied the NF_2 absorption as a function of temperature. We observed no change of the cross section within our experimental error of 10% for temperatures from 400 to 500 K. Thus the dependence observed in Ref. 23 is probably caused by the $\text{N}_2\text{F}_4/\text{NF}_2$ equilibrium¹⁷⁻²³ rather than the NF_2 ground state population distribution. From these experiments, we determined the NF_2 absorption cross section at the KrF wavelength to be $(6.1 \pm 0.6) \times 10^{-19}$ cm². There is a discrepancy among the published values for the NF_2 absorption coefficients at 260 nm, which is summarized in Ref. 18. This variation may be due to insufficiently monochromatic sources used in some studies which would tend to average the structure in the 260 nm absorption band. Within the uncertainty in the temperature dependence of the NF_2 260 nm band contour,^{22,23} our value of the absorption coefficient at 249 nm agrees best with that of Ref. 22.

The first order deactivation of $\text{NF}(a)$ by various collision partners has been studied by Kwok and Herbelin¹⁰ and Cheah and Clyne.¹⁶ Their qualitative results indicate that deactivation is slow with such partners as H_2 , HF , D_2 , and NF_2 . In a set of experiments, we investigated the quenching of $\text{NF}(a)$ by the parent molecule NF_2 . The observation of slow $\text{NF}(a)$ decays from photolysis

of NF_2/Ar mixtures (Fig. 2) confirms that NF_2 is an inefficient quencher of NF(a) . Examination of the NF(a) decay as a function of NF_2 results in a value of $(2.7 \pm 0.8) \times 10^{-16} \text{ cm}^3/\text{molecule-sec}$ for the quenching rate constant. These data are presented in Fig. 5. The nonzero intercept is caused by the effects of NF(a) diffusion to the walls. Although the diffusion coefficient of NF(a) in Ar is not known, if one uses the value for O_2 in Ar ($0.392 \text{ cm}^2/\text{sec-atm}$), a radial diffusion rate of 17 sec^{-1} is obtained for these experimental conditions. This is in reasonable agreement with the intercept value of $23 \pm 4 \text{ sec}^{-1}$.

It has been suggested that a rapid bimolecular disproportionation occurs between two ground state NF molecules^{9,14} in reaction (5). There is no direct experimental evidence that disproportionation occurs rapidly between excited states of NF;¹⁶ indeed there are spin conservation arguments against such a process.⁹ This question bears upon the interpretation of the data presented in Fig. 5 since NF(a) scales linearly with NF_2 using constant photolysis intensity. In a set of separate experiments, NF(a) decays were measured as a function of $[\text{NF(a)}]$, with $[\text{NF}_2]$ held constant. This was accomplished by a variation of the photolysis intensity on an NF_2/Ar mixture. The initial NF(a) was varied over two orders of magnitude, and the results of this experiment are plotted in Fig. 6. NF(a) densities are calculated using a 10% quantum yield (see Section IIID). Although NF(a) disproportionation is not a first-order process, from the slope in Fig. 6 we can obtain an estimate for this rate of $(4 \pm 3) \times 10^{-14} \text{ cm}^3/\text{molecule-sec}$.

It should be noted that if the abscissa in Fig. 5 is converted to NF(a) density using the photolysis fraction, the value of the slope, $1.2 \times 10^{-12} \text{ cm}^3/\text{molecule-sec}$, is inconsistent with the rate coefficient obtained from Fig. 6. The value suggested for $\text{NF(a)} + \text{NF(a)}$ [$(4 \pm 3) \times 10^{-14} \text{ cm}^3/\text{molecule-sec}$] is three orders of magnitude smaller than the overall removal rate for NF radicals ($7 \times 10^{-11} \text{ cm}^3/\text{molecule-sec}$).¹⁴

B. THREE-BODY RECOMBINATION OF F WITH NF_2

To determine the NF(a) photolysis quantum yield from NF_2 at 249 nm, it was our intention to perform the necessary absolute calibration of our

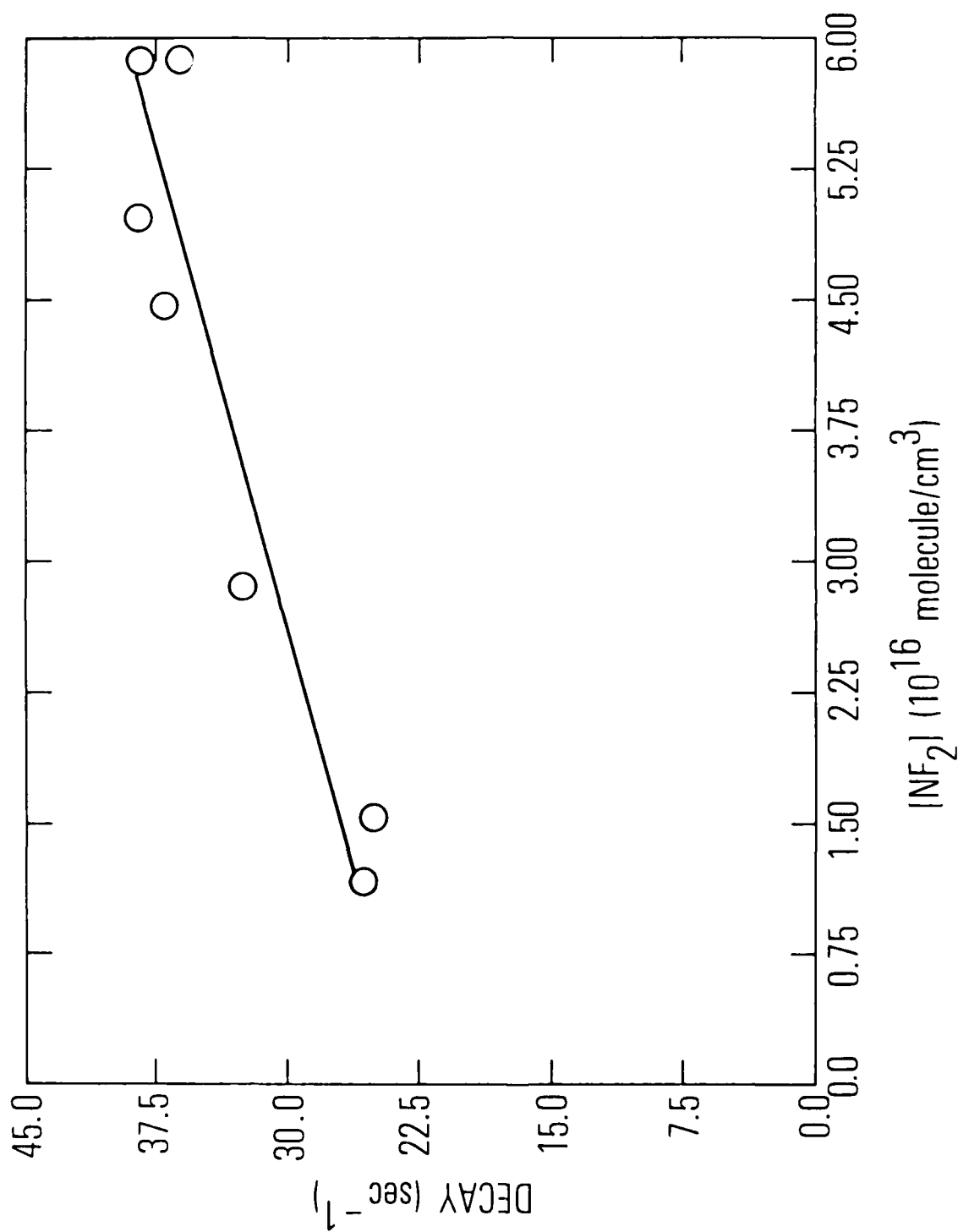


Fig. 5. $\text{NF}_2 + \text{X}$ Fluorescence Decay from Photolysis of NF_2/Ar Mixtures vs. $[\text{NF}_2]$. Also shown is a linear fit to the data.

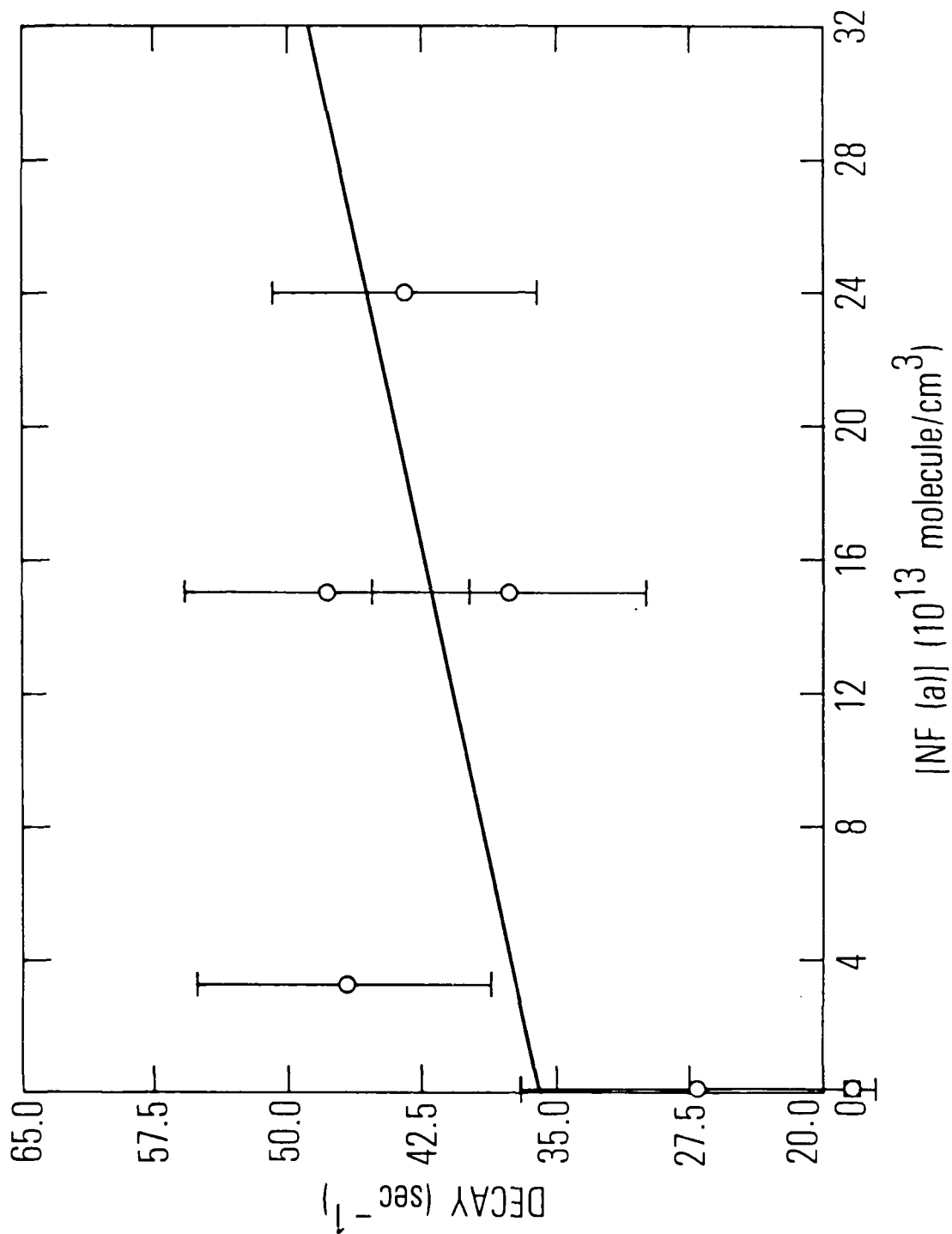


Fig. 6. NF a - X Emission Decay as a Function of [NF(a)]. The NF₂ density was held constant, and the photolysis flux was varied. [NF(a)] was calculated using an absorption cross section of 6.1×10^{-19} cm² and an NF(a) photolysis quantum yield of 10%.

detection sensitivity to NF(a) by titrating the F atoms produced in the photolysis with H₂. This would provide an internal calibration, since each F + H₂ reaction results in one hydrogen atom, a known fraction of which forms NF(a) via reaction (4).⁸ However, this approach yielded results unlike typical gas phase titration curves (see Section IIIC and Fig. 10). This led us to suspect that there was another process competing with reaction (2) for F atoms. A likely candidate under our experimental conditions of relatively high Ar density, $\sim 10^{17}$ molecule/cm³, is reaction (3), the three-body recombination of NF₂ with fluorine atoms. The observation that NF(a) amplitudes from photolysis of NF₂/H₂/Ar mixes depended upon the Ar density confirmed this suspicion. An analytic model was developed to enable extraction of the recombination rate coefficient, k₃, from the NF(a) behavior. The derivation of this model is given in Appendix A. The treatment neglects deactivation of NF(a) and is concerned with the short-time formation of NF(a). This is a reasonable assumption since the formation and decay of NF(a) in this study occur under extremely different time scales. In addition, only reactions (2) through (5) are considered, and NF(X) and NF(b) produced from reaction (4) are neglected. The explicit integration of the rate equations restricts the range of validity of this model. The [H₂]/[F] ratio must be large so that [H₂] may be taken as a constant. Furthermore, there must be sufficient NF₂ to ensure that the time behavior of NF(a) from reaction (4) and H from reaction (2) will be identical. In this study, the rate of reaction (2) was a factor of 2 slower than reaction (4) at the highest H₂ density. Thus the assumption that the NF(a) density parallels that of H atoms is good. Under these constraints, we arrive at the expression:

$$NF(a) = \frac{bF_0}{a} (1 - e^{-at}) + \frac{bcNF(X)_0}{a} \left[\frac{t}{(1 + ct)} - B(t)e^{-at} \right] \quad (8)$$

where $B(t) = \int_0^t e^{at'} / (1 + bt')^2 dt'$, $a = k_2[H_2] + k_3[NF_2][Ar]$, $b = k_1[H_2]$, and $c = k_5[NF(X)_0]$. Hence, this model predicts that the NF(a) formation is not a simple single exponential because of the additional source of F atoms

from reaction (5). From Eq. (8) we can obtain a simple expression for the NF(a) amplitudes:

$$NF(a) = b/a [F_0 + NF(X)_0]. \quad (9)$$

From this we see that of the available fluorine atoms, $[F_0 + NF(X)_0]$, the amount that appears in the NF(a) product is given by the branching fraction c/a . This explains our observation that the NF(a) amplitudes depend upon $[Ar]$. The atypical F atom titration data are due to competition for F atoms by reactions (2) and (3).

Equation (9) was exploited to obtain k_3 . In a series of runs, the partial pressure of Ar was varied, whereas $[H_2]$ and $[NF_2]$ were held fixed at 8.2×10^{13} and 9.0×10^{15} molecule/cm³, respectively. The KrF laser flux was 7.9×10^{15} photons/cm³ resulting in an initial F atom concentration of 2.1×10^{13} molecule/cm³. The KrF beam was expanded to fill the cell as nearly as possible so that diffusion effects were minimized. From Eq. (9) it follows that the inverse of the observed NF(a) amplitude is linear with respect to $[Ar]$:

$$1/[NF(a)] = \{k_3[NF_2]/S[F]_{av} k_2[H_2]\}[Ar] + 1/S[F]_{av}, \quad (10)$$

where $[F]_{av}$ represents the available F atoms, $[F_0] + [NF(X)_0]$, and S is a constant defining the absolute NF(a) detection sensitivity. A plot of the data and a linear fit are shown in Fig. 7. The NF(a) amplitudes used in Fig. 7 were obtained from a nonlinear least squares fit of the NF(a) time profiles to a double exponential, $[NF(a)] = c_1[e^{-c_2t} - e^{-c_3t}]$, to obtain NF(a) amplitudes. The value of k_3 extracted from the linear fit is $(1.0 \pm 0.3) \times 10^{-30}$ cm⁶/molecule²-sec using the value of k_2 at 440 K from Ref. 27.

In actuality, the NF(a) profiles are truly represented by Eq. (8) rather than a double exponential. However, the formation and decay of NF(a) occur on such a different time scale that amplitudes from such fits agree within experimental error with the measured NF(a) maxima. If the rising part of the NF(a) profiles is neglected and the decays are fitted to a single exponential function, the amplitudes from an extrapolation to $t = 0$ also agree.

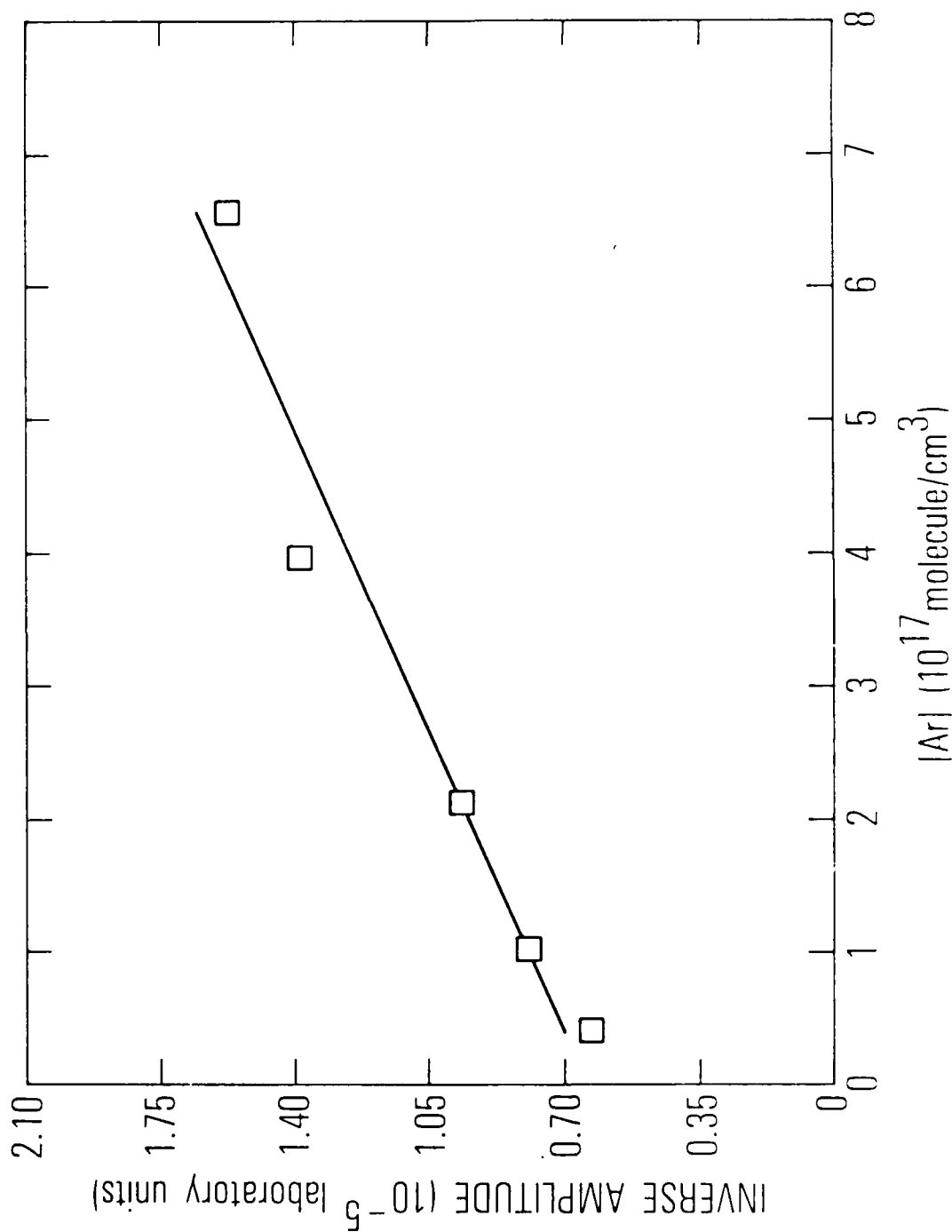


Fig. 7. Plot of NF(a) Amplitudes vs. [Ar] According to Eq. (3). H_2 and NF_2 densities were held fixed at 8.2×10^{13} and 9.0×10^{15} molecule/cm 3 , respectively. KrF laser flux was 7.9×10^{15} photons/cm 2 resulting in an initial F atom concentration of 2.1×10^{13} molecule/cm 3 . A linear fit is indicated as well.

In addition to providing amplitudes, the double exponential fits allow a qualitative estimate of the dependence of the risetime on $[H_2]$ or $[Ar]$. This is discussed further in Section IIIC.

In a similar manner, the $NF(a)$ intensity was measured with respect to $[H_2]$, while keeping the density of other species constant. An equation similar to Eq. (10) may be obtained from Eq. (9):

$$1/[NF(a)] = \{k_3[NF_2][Ar]/k_2S[F]_{av}\}/[H_2] + 1/S[F]_{av}, \quad (11)$$

showing that the inverse of $NF(a)$ is proportional to $1/[H_2]$. A set of data in accordance with Eq. (11) is shown in Fig. 8. From these data, a value of $(1.1 \pm 0.2) \times 10^{-30} \text{ cm}^6/\text{molecule}^2\text{-sec}$ is obtained for k_3 .

An experimental determination of $(8.9 \pm 3.3) \times 10^{-31} \text{ cm}^6/\text{molecule}^2\text{-sec}$ for the rate constant for recombination of NF_2 and F atoms in He at 300 K has been performed by Clyne and Watson.²⁹ A recent theoretical study^{30,31} indicates that this magnitude of the rate constant should scale inversely with the mass of the rare gas partner and the temperature. The discrepancy between our value for k_3 , and this trend predicted in Ref. 30, indicates that further work is needed to resolve this question. However, the agreement between the intercepts in Figs. 7 and 8 $(6.3 \pm 0.9) \times 10^{-6}$ and $(5.2 \pm 0.8) \times 10^{-6}$ lab units, respectively, provides evidence that the method used here to obtain the recombination rate constant is valid. Further confirmation is presented in the following paragraphs.

C. COMPUTER MODEL OF THE NF_2/H_2 SYSTEM

To provide additional confirmation of the analytic model and to understand the $NF(a)$ kinetics under conditions where the assumptions used in its derivation are not met, a computer model of the system was constructed using the NEST computer code.³² A total of 35 reactions were included and are listed in Appendix B. Rate constants at 440 K were used whenever possible. The experimental $NF(a)$ profiles obtained from photolysis of the $NF_2/Ar/H_2$ mixtures used to produce Fig. 8 were modeled. Fluorine-rich conditions were

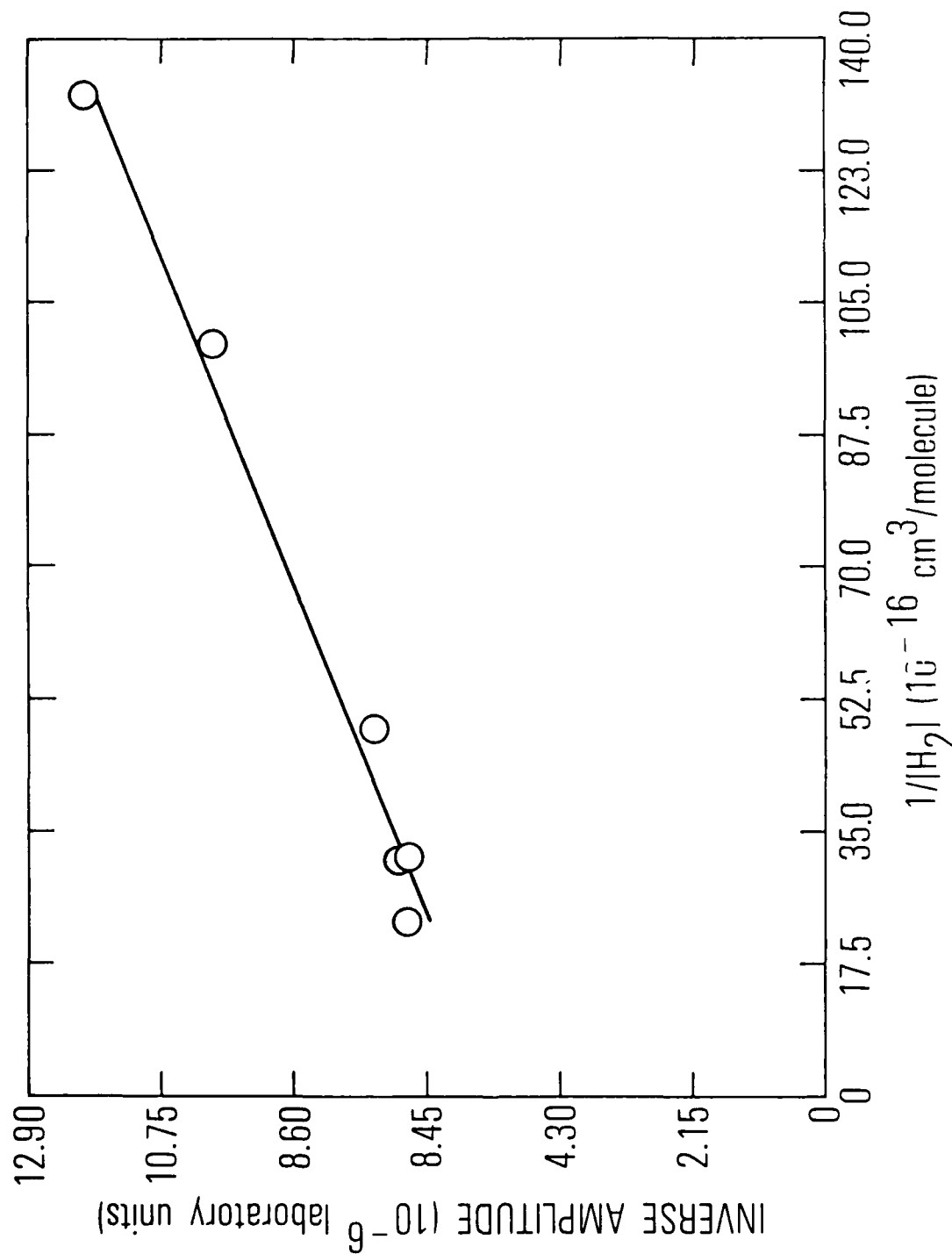


Fig. 8. Plot of NF(a) Amplitudes vs. $[H_2]$ According to Eq. (4). Ar and NF₂ densities were held fixed at 4.0×10^{17} and 9.7×10^{15} molecule/cm³, respectively. KrF laser flux was 7.9×10^{15} photons/cm² resulting in an initial F atom concentration of 2.3×10^{13} molecule/cm³. A linear fit is indicated as well.

also treated, which are out of the range of validity of Eq. (8). Good agreement was obtained with this computer model for $[H_2]$ ranging from 3×10^{12} to 4×10^{14} molecule/cm³. A comparison of the computer and analytic model with the experiment is shown in Fig. 9. The integral function, $B(t)$, that appears in Eq. (1) was evaluated using the Simpson method.

Because of the competition for fluorine atoms by reaction (3), absolute calibration of our detection sensitivity to $NF(a)$ using an H_2 titration of F atoms is precluded. Instead, we effected this calibration using the modeling results in conjunction with experimental data. Experimental $NF(a)$ profiles were obtained for 11 H_2 concentrations, keeping the Ar and NF_2 densities fixed. Photolysis flux remained constant to ensure that initial F, $NF(a)$, and $NF(X)$ densities did not vary. The H_2 density was varied from 3×10^{12} to 4×10^{14} molecule/cm³. NEST was used to simulate the $NF(a)$ behavior for each case. The NEST output was fitted to a double exponential in the same manner as the experimental data. The resulting $NF(a)$ amplitudes were plotted as a function of $[H_2]$ for both experiment and model. The results are depicted in Fig. 10. Best agreement is obtained using a scaling factor of 2.13×10^8 to convert laboratory $NF(a)$ amplitude units to absolute number densities.

To test the analytic model and obtain the scaling factor independently, the calculated NEST data shown in Fig. 10 were plotted in the same manner as the data shown in Fig. 8, subject to the restrictions that $[H_2]$ exceeds $[F]$. From the slope of such a plot (not shown), a value of $k_3 = 1.0 \times 10^{-30}$ cm⁶/molecule²-sec was extracted from the NEST calculation. This exactly reproduces the value input into the NEST code, giving strong evidence that the methodology of Section IIIB is valid. According to Eq. (11), the sum of the initial F and $NF(X)$ densities is given by the intercept of this plot. A value of 4.03×10^{13} molecule/cm³ is obtained, which is somewhat different from the NEST input value of 5.2×10^{13} . This discrepancy results primarily because the analytic model neglects the $NF(a)$ pooling with vibrationally excited HF, indicated in reaction (7). In fact, the NEST model predicts that the $NF(b)$ density is on the order of 15% of $[NF(a)]$, which is in semiquantitative agreement with experimental results.

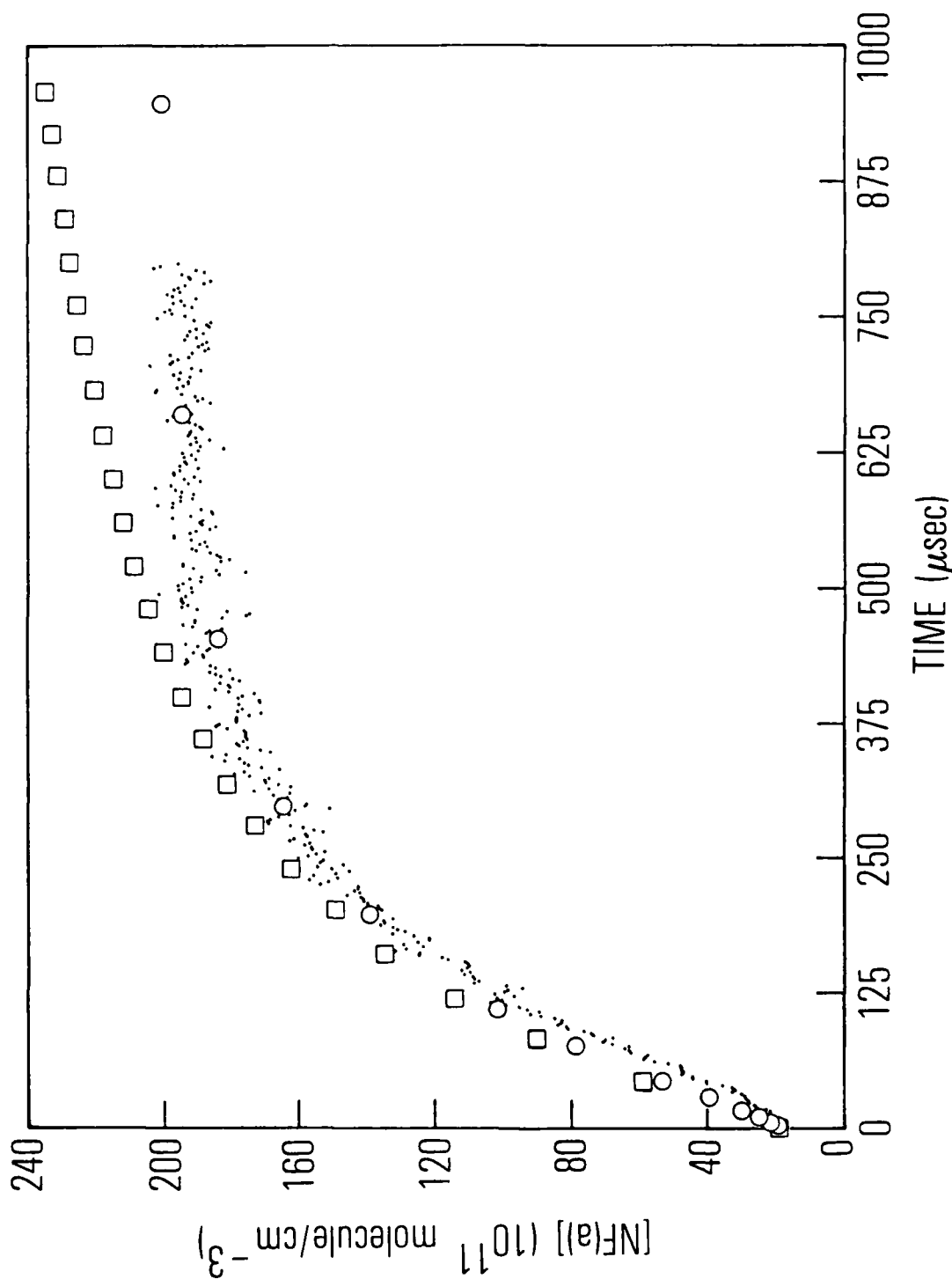


Fig. 9. Formation Behavior of NF(a) from KrF Photolysis of an NF₂/H₂/Ar Mix. The points are the experimental data whereas the squares and circles represent the analytic and NEST model, respectively. Experimental data are scaled to absolute densities using absolute calibration factor (see Section III). [Ar] = 4.0×10^{17} , [NF₂] = 9.7×10^{15} , [H₂] = 1.0×10^{14} , [F] = 2.6×10^{13} , [NF(a)] = 2.6×10^{12} , [NF(X)] = 2.3×10^{13} . The slow NF(a) decay rate was included in the NEST model phenomenologically.

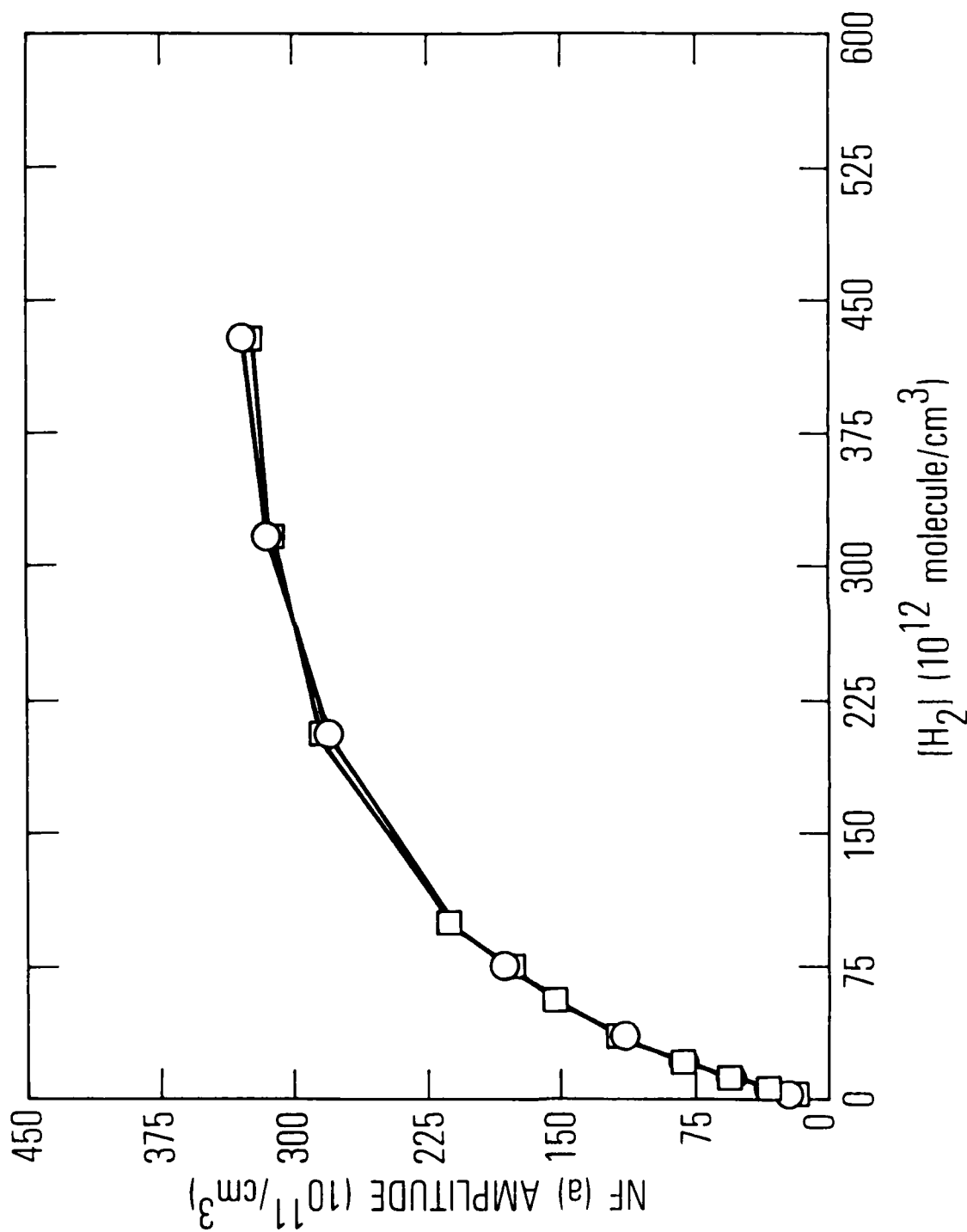


Fig. 10. NF(a) Amplitudes as a Function of $[H_2]$. NEST data are given by the circles, and the experimental results are the squares. The scaling factor for the data to give the best agreement is 2.13×10^8 lab units/molecule cm^{-3} .

It is interesting to examine the variation of the NF(a) "risetimes" obtained from the double exponential fits as a function of $[H_2]$. Risetimes from the experimental data and from the NEST calculation are displayed in Fig. 11. Satisfactory agreement is observed except for the two lowest $[H_2]$ concentrations. However, the qualitative behavior is well represented by the NEST treatment. This provides further evidence that the NEST model is valid.

D. NF(a) QUANTUM YIELD

The observed and modeled dependence of the NF(a) amplitudes upon $[H_2]$, presented in Sections IIIB and IIIC, allowed us to obtain an absolute calibration of our NF(a) detection sensitivity. Under identical conditions of detection geometry and KrF laser flux used in the above titration study, the NF(a) amplitude from the photolysis of NF_2 was determined in the absence of H_2 . Using previously discussed absolute calibration factors, the photolysis of 9.67×10^{15} molecule/cm³ of NF_2 resulted in an NF(a) density of 2.9×10^{12} . This represents a quantum yield of $(10 \pm 5)\%$, using our NF_2 absorption cross section and the measured KrF power density. The estimated uncertainty results mainly from the uncertainty in the amplitude-to-concentration calibration factor. This value for the quantum yield was calculated assuming that the dissociation quantum yield for Process (1) is unity.

As noted previously, the NF(a) appears on a time scale much longer (~ 5 μ sec) than the KrF photolysis pulse (~ 15 nsec), and this appearance rate is independent of $[NF_2]$. Therefore, some short-lived intermediate state may be involved in the dissociation process. Nevertheless, the agreement between the models and the experimental data discussed above indicates that reaction (1) does proceed with a quantum efficiency near unity.

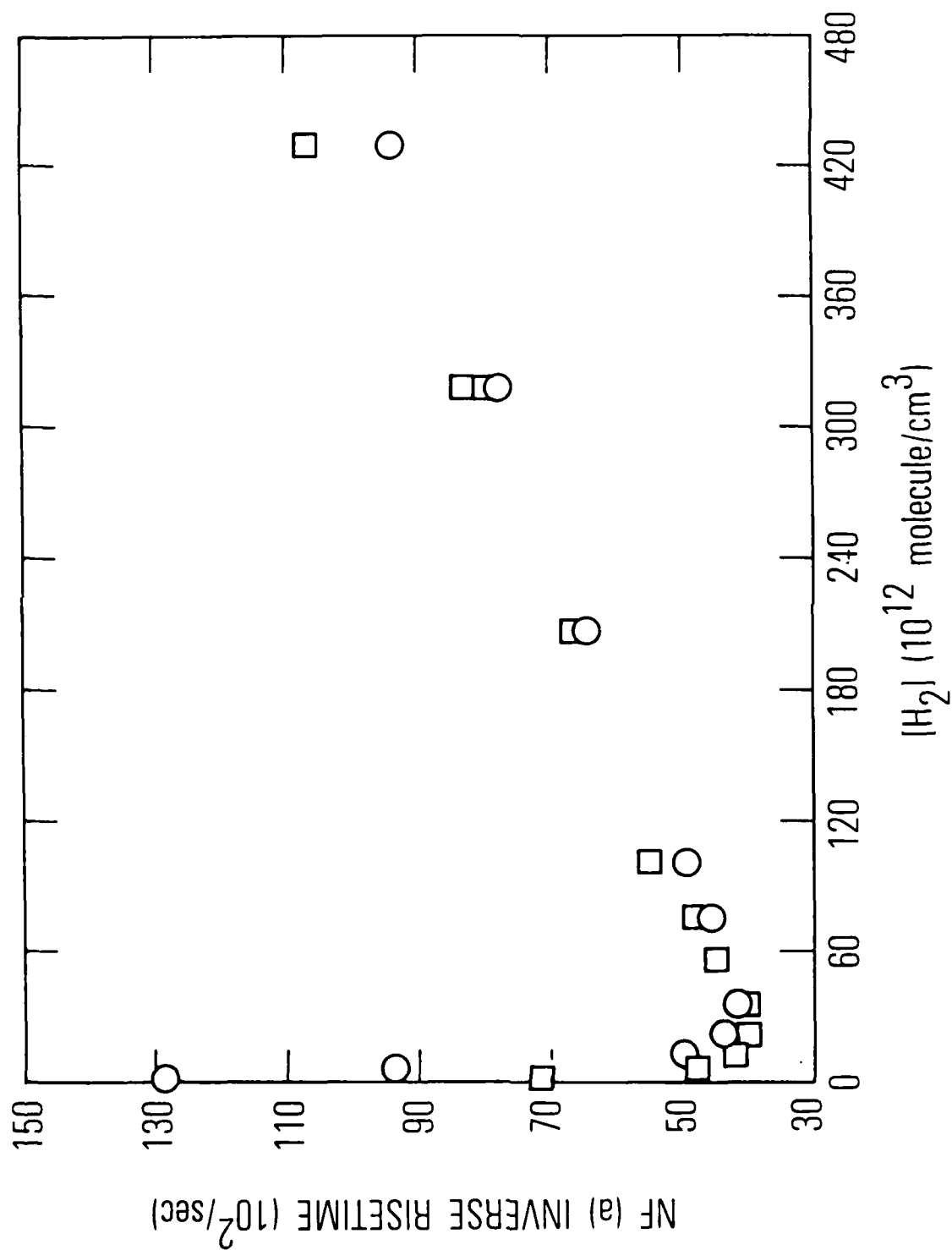


Fig. 11. NF(a) Risetimes as a Function of [H₂]. The experimental points are given by the squares, and the circles are the result of the NEST calculations.

IV. CONCLUSIONS

The kinetics of NF(a) formation from the KrF laser-initiated reaction of NF₂/H₂/Ar mixtures were determined. The quenching rates of NF(a) as well as HF(v = 2 and 3) by NF₂ have been measured. Good agreement exists between experimental data and analytic and computer models of the system presented here. The three-body recombination of NF₂ with F atoms has been studied, and the rate constant has been extracted from the data using the results of a simple analytic model. Evidence suggests that this treatment of the data is valid, however, the results are not in agreement with a previous study.^{30,31} Further work is needed to resolve this discrepancy.

The NF(a) time profiles from the photolysis of NF₂/Ar mixtures displayed short risetimes, which may suggest that some intermediate state exists during the photolytic process. Although the modeling results indicate that the quantum yield for NF₂ dissociation into an NF radical and a fluorine atom is near unity, the cause of the NF(a) risetime remains unknown. The observation of HF(v = 2 and 3) following photolysis of NF₂/Ar mixtures indicates the presence of a hydrogen-bearing impurity. However, strong evidence was obtained that HF is produced from the reaction of F atoms with an impurity hydrocarbon (or possibly HNF₂), a channel that would not lead to NF(a). Thus, this impurity does not affect the NF(a) photolysis quantum yield at 249 nm reported in this work.

Experiments are planned to examine the NF(b) state kinetics and to extend the kinetics of this interesting reaction system into the region of high radical species densities where second order processes will be important. In addition, the cause of the NF(a) risetime from NF₂ photolysis alone will be investigated.

REFERENCES

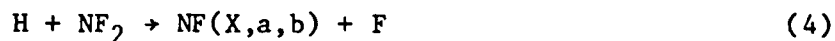
1. M. A. A. Clyne and I. F. White, Chem. Phys. Lett. 6, 465 (1970).
2. T. D. Padrick and G. C. Pimentel, J. Chem. Phys. 54, 720 (1971).
3. L. E. Brus and M. C. Lin, J. Phys. Chem. 75, 2546 (1971).
4. R. J. Collins and D. Husain, J. Photochem. 2, 459 (1972).
5. Yu. M. Gershenzon, S. D. Il'in, O. P. Kishkovitch, R. T. Malkhasyan, V. B. Rozenshtein, and S. Ya. Umanskii, Int. J. Chem. Kinet. 15, 399 (1983).
6. Yu. M. Gershenzon, S. D. Il'in, S. A. Kolesnikov, Ya. S. Lebedev, R. T. Malkhasyan, A. B. Nalbandyan, and G. R. Trubnikov, Kinet. Katal. 23, 534 (1982).
7. J. M. Herbelin and N. Cohen, Chem. Phys. Lett. 20, 605 (1973).
8. R. J. Malins and D. W. Setser, J. Phys. Chem. 85, 1342 (1981).
9. J. M. Herbelin, Chem. Phys. Lett. 42, 367 (1976).
10. M. A. Kwok and J. M. Herbelin, "Electronic Transition Lasers II," L. E. Wilson, S. N. Suchard, and J. I. Steinfeld (editors), MIT Press, Boston (1977).
11. J. M. Herbelin, M. A. Kwok, and N. Cohen, Technical Report, TR-0081(6610)-1, The Aerospace Corp., El Segundo, Calif. (1981).
12. J. M. Herbelin, M. A. Kwok, and N. Cohen, Technical Report, TR-0077(2940)-6, The Aerospace Corp., El Segundo, Calif. (1977).
13. P. H. Tennyson, A. Fontijn, and M. A. A. Clyne, Chem. Phys. 62, 171 (1981).
14. C. T. Cheah, M. A. A. Clyne, and P. D. Whitefield, J. Chem. Soc. Faraday Trans. II 76, 711 (1980).
15. C. T. Cheah and M. A. A. Clyne, J. Chem. Soc. Faraday Trans. II 76, 1543 (1980).
16. C. T. Cheah and M. A. A. Clyne, J. Photochem. 15, 21 (1981).
17. P. J. Evans and E. Tschuikow-Roux, J. Phys. Chem. 82, 182 (1978).
18. P. J. Evans and E. Tschuikow-Roux, J. Chem. Phys. 10, 4202 (1976).

19. S. N. Foner and R. L. Hudson, J. Chem. Phys. 58, 581 (1973).
20. A. P. Modica and D. F. Hornig, J. Chem. Phys. 49, 629 (1968).
21. F. A. Johnson and C. B. Colburn, J. Am. Chem. Soc. 83, 3043 (1961).
22. P. L. Goodfriend and H. P. Woods, J. Mol. Spectrosc. 13, 63 (1964).
23. L. A. Kuznetsova, Yu. Ya. Kuzyakov, and T. M. Tatevskii, Optics Spectrosc. 16, 295 (1964).
24. J. T. Herron and V. H. Diebler, J. Chem. Phys. 33, 1595 (1960).
25. A. E. Douglas and W. E. Jones, Can. J. Phys. 45, 21 (1967).
26. B. de B. Darwent, NSRDS 31 (1970).
27. N. Cohen and J. F. Bott, Technical Report, TR-0083(3603)-2, The Aerospace Corp., El Segundo, Calif. (1983).
28. D. G. Imre, J. L. Kinsey, R. W. Field, and D. H. Kayatama, 7th International Symposium on Gas Kinetics, Gottingen (1982).
29. M. A. A. Clyne and R. T. Watson, J. Chem. Soc. Faraday Trans. I 70, 1109 (1974).
30. G. P. Smith and D. L. Huestis, J. Appl. Phys. 52, 6041 (1981).
31. K. Y. Tang, R. O. Hunter, Jr., and D. L. Huestis, J. Appl. Phys. 52, 6046 (1981).
32. E. B. Turner, G. Emanuel, and R. L. Wilkins, Technical Report, TR-0059(6240-20)-1, The Aerospace Corporation, El Segundo, Calif. (1970).

APPENDIX A

NF(a) KINETIC MODEL

The reactions considered in this model are:



In addition, the NF(X) and NF(b) produced from reaction [4] are neglected. One can explicitly integrate the differential equation for NF(X),

$$[\dot{NF}(X)] = -k_5[NF(X)]^2, \quad (A1)$$

to give

$$[NF(X)] = [NF(X)]_0 / (1 + k_5[NF(X)]_0 t), \quad (A2)$$

where $[NF(X)]_0$ is the initial NF(X) concentration. The equation for fluorine is written as

$$[\dot{F}] = -\{k_2[H_2] + k_3[NF_2][Ar]\}[F] + k_5[NF_2]^2 \quad (A3)$$

Using Eq. (A2), Eq. (A3) is given by

$$[\dot{F}] = -a[F] + c[NF(X)]_0 / [(1 + ct)^2] \quad (A4)$$

where $a = k_2[H_2] + k_3[NF_2][Ar]$ and $c = k_5[NF(X)]_0$. Under conditions of excess H_2 and NF_2 so that a is constant, Eq. (A4) is of the form

$$\dot{Y} + kY = f(t), \quad (A5)$$

for which the solution is

$$Y(t) = e^{-kt}F(t) + Ce^{-kt}, \quad (A6)$$

where C is an integration constant and $F(t)$ is

$$F(t) = \int_0^t e^{-kt'} f(t') dt' \quad (A7)$$

Using Eqs. (A6) and (A7), we can write the solution for the F atom time dependence as

$$[F] = [F]_0 e^{-at} + c[NF(X)]_0 B(t) e^{-at}, \quad (A8)$$

where $[F]_0$ is the initial F atom density and $B(t)$ is given by

$$B(t) = \int_0^t e^{at'} / [(1 + ct')^2] dt' \quad (A9)$$

Under conditions of high $[NF_2]$ where reaction (4) proceeds rapidly with respect to reaction (2), the formation rate of $NF(a)$ is equal to the H atom production rate in reaction (2) and is given by

$$[\dot{NF}(a)] = b[F] \quad (A10)$$

where $b = k_2[H_2]$. Equations (A8) through (A10) lead to an equation for $NF(a)$ as follows:

$$[\dot{NF}(a)] = bc[NF(X)]_0 \{e^{-at} B(t) + [F]_0 e^{-at}\}, \quad (A11)$$

which upon integration leads to

$$[NF(a)] = b[F]_0 / (a[1 - e^{-at}] + bc[NF(X)]_0 \int_0^t e^{-at'} B(t') dt') \quad (A12)$$

The second term in Eq. (A12) can be integrated by parts to obtain the result presented in the text:

$$[NF(a)] = \frac{bF_0}{a} [1 - e^{-at}] + \frac{bc[NF(X)]_0}{a} \left[\frac{c}{(1 + ct)} - B(t)e^{-at} \right]$$

APPENDIX B

REACTIONS USED IN THE NEST MODEL

Reaction	k (cm ³ /molecule-sec)	Reference
F + H ₂ → HF(1) + H	7.3 × 10 ⁻¹²	(26)
F + H ₂ → HF(2) + H	2.4 × 10 ⁻¹¹	(26)
F + H ₂ → HF(3) + H	1.2 × 10 ⁻¹¹	(26)
H + NF ₂ → HF(0) + NF(a)	8.0 × 10 ⁻¹²	(8)
H + NF ₂ → HF(1) + NF(a)	3.0 × 10 ⁻¹²	(8)
H + NF ₂ → HF(2) + NF(a)	7.7 × 10 ⁻¹³	(8)
H + NF ₂ → HF(3) + NF(a)	1.2 × 10 ⁻¹³	(8)
H + NF ₂ → HF(0) + NF(b)	2.6 × 10 ⁻¹³	(8)
H + NF ₂ → HF(0) + NF(X)	9.1 × 10 ⁻¹³	(8)
H + NF(a) → HF(0) + N(² D)	2.5 × 10 ⁻¹³	(15),(16)
H + NF(b) → H + NF(a)	5 × 10 ⁻¹²	(12)
HF(2) + NF(a) → NF(b) + HF(0)	8.3 × 10 ⁻¹²	(11)
HF(3) + NF(a) → NF(b) + HF(1)	7.5 × 10 ⁻¹¹	a
HF(4) + NF(a) → NF(b) + HF(2)	3.3 × 10 ⁻¹²	a
N(² D) + NF(a) → N ₂ (B,a) + F	3.0 × 10 ⁻¹¹	(16)
NF(X) + NF(X) → N ₂ (X) + 2F	7 × 10 ⁻¹¹	(14)
NF(a) + NF(a) → N ₂ (X) + 2F	≤ 1 × 10 ⁻¹³	This work
HF(1) + HF(1) → HF(0) + HF(2)	1.7 × 10 ⁻¹¹	(26)
HF(1) + HF(2) → HF(0) + HF(3)	2.0 × 10 ⁻¹¹	(26)
HF(1) + HF(3) → HF(4) + HF(0)	2.2 × 10 ⁻¹¹	(26)
HF(4) + HF(0) → HF(3) + HF(0)	4.3 × 10 ⁻¹¹	(26)
HF(3) + HF(0) → HF(2) + HF(0)	2.0 × 10 ⁻¹¹	(26)
HF(2) + HF(0) → HF(1) + HF(0)	7.2 × 10 ⁻¹²	(26)
HF(1) + HF(0) → HF(0) + HF(0)	1.2 × 10 ⁻¹²	(26)
HF(4) + H ₂ → HF(3) + H ₂	8.5 × 10 ⁻¹³	(26)
HF(3) + H ₂ → HF(2) + H ₂	3.9 × 10 ⁻¹³	(26)
HF(2) + H ₂ → HF(1) + H ₂	1.3 × 10 ⁻¹³	(26)
HF(1) + H ₂ → HF(0) + H ₂	2.0 × 10 ⁻¹⁴	(26)
HF(1) + NF ₂ → HF(0) + NF ₂	1.4 × 10 ⁻¹⁴	b
HF(2) + NF ₂ → HF(1) + NF ₂	9.7 × 10 ⁻¹⁴	This work
HF(3) + NF ₂ → HF(2) + NF ₂	2.5 × 10 ⁻¹³	This work
HF(4) + NF ₂ → HF(3) + NF ₂	5.8 × 10 ⁻¹³	b
NF(b) → NF(X) + hν	45	(12),(13),(16) ^c
F + NF ₂ + Ar → NF ₃ + Ar	1.0 × 10 ⁻³⁰	This work ^d
NF(a) + NF ₂ → NF(X) + NF ₂	2.7 × 10 ⁻¹⁶	This work

^aEstimated.^bCalculated using v^{2.7} power law.^cUnits of sec⁻¹.^dUnits of cm⁶/molecule²-sec.PREVIOUS PAGE
IS BLANK

LABORATORY OPERATIONS

The Laboratory Operations of The Aerospace Corporation is conducting experimental and theoretical investigations necessary for the evaluation and application of scientific advances to new military space systems. Versatility and flexibility have been developed to a high degree by the laboratory personnel in dealing with the many problems encountered in the nation's rapidly developing space systems. Expertise in the latest scientific developments is vital to the accomplishment of tasks related to these problems. The laboratories that contribute to this research are:

Aerophysics Laboratory: Launch vehicle and reentry fluid mechanics, heat transfer and flight dynamics; chemical and electric propulsion, propellant chemistry, environmental hazards, trace detection; spacecraft structural mechanics, contamination, thermal and structural control; high temperature thermomechanics, gas kinetics and radiation; cw and pulsed laser development including chemical kinetics, spectroscopy, optical resonators, beam control, atmospheric propagation, laser effects and countermeasures.

Chemistry and Physics Laboratory: Atmospheric chemical reactions, atmospheric optics, light scattering, state-specific chemical reactions and radiation transport in rocket plumes, applied laser spectroscopy, laser chemistry, laser optoelectronics, solar cell physics, battery electrochemistry, space vacuum and radiation effects on materials, lubrication and surface phenomena, thermionic emission, photosensitive materials and detectors, atomic frequency standards, and environmental chemistry.

Computer Science Laboratory: Program verification, program translation, performance-sensitive system design, distributed architectures for spaceborne computers, fault-tolerant computer systems, artificial intelligence and microelectronics applications.

Electronics Research Laboratory: Microelectronics, GaAs low noise and power devices, semiconductor lasers, electromagnetic and optical propagation phenomena, quantum electronics, laser communications, lidar, and electro-optics; communication sciences, applied electronics, semiconductor crystal and device physics, radiometric imaging; millimeter wave, microwave technology, and RF systems research.

Materials Sciences Laboratory: Development of new materials: metal matrix composites, polymers, and new forms of carbon; nondestructive evaluation, component failure analysis and reliability; fracture mechanics and stress corrosion; analysis and evaluation of materials at cryogenic and elevated temperatures as well as in space and enemy-induced environments.

Space Sciences Laboratory: Magnetospheric, auroral and cosmic ray physics, wave-particle interactions, magnetospheric plasma waves; atmospheric and ionospheric physics, density and composition of the upper atmosphere, remote sensing using atmospheric radiation; solar physics, infrared astronomy, infrared signature analysis; effects of solar activity, magnetic storms and nuclear explosions on the earth's atmosphere, ionosphere and magnetosphere; effects of electromagnetic and particulate radiations on space systems; space instrumentation.

END

FILMED

12-85

DTIC